

# Computer Simulation of Gas-Phase Neutralization of Electrospray-Generated Protein Macroions

Igor L. Kanev,<sup>†</sup> Nikolay K. Balabaev,<sup>‡,§</sup> Anna V. Glyakina,<sup>‡</sup> and Victor N. Morozov<sup>\*,†,||</sup>

<sup>†</sup>Institute of Theoretical and Experimental Biophysics, Russian Academy of Sciences, Pushchino, Moscow Region, Russia 142290

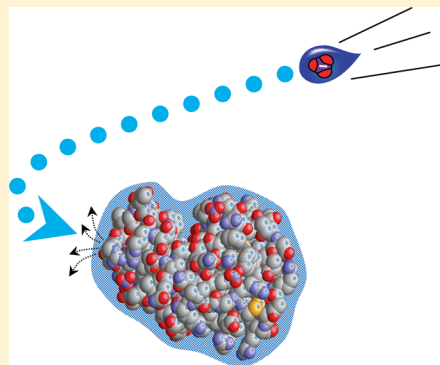
<sup>‡</sup>Institute of Mathematical Problems of Biology, Russian Academy of Sciences, Pushchino, Moscow Region, Russia 142290

<sup>§</sup>Department of Bioengineering, Faculty of Biology, M.V. Lomonosov Moscow State University, Moscow, Russia 119991

<sup>||</sup>The National Center for Biodefense and Infectious Diseases, George Mason University, Manassas, Virginia 20110, United States

## S Supporting Information

**ABSTRACT:** The process of neutralizing hydrated multicharged gas-phase protein ions with small counterions was simulated using a molecular dynamics (MD) technique. Hen egg white lysozyme (HEWL) molecules with different numbers of positive charges, both dry and solvated by up to 1500 water molecules, were first equilibrated. Simulations revealed that the hydration layer over a highly charged protein surface adapted a spiny structure with water protrusions composed of oriented water dipoles. MD simulations of the neutralization process showed that the impact of a small dehydrated single-charged counterion with a dehydrated HEWL ion bearing eight uncompensated charges resulted in a short local increase in temperature by 600–1000 K, which quickly (in 3–5 ps) dissipated over the whole protein molecule, increasing its average temperature by 20–25 K. When the protein ion was solvated, no drastic local increase in the temperature of the protein atoms was observed, because the impact energy was dissipated among the water molecules near the collision site.



## INTRODUCTION

Gas-phase neutralization of electrospray-generated products is employed both in research and in commercial devices. The process is exploited in nanoaerosol generators used for the calibration of aerosol spectrometers (Grimm Technologies Inc., Douglasville, GA, and TSI, Inc., St. Paul, MN, USA). It is also employed in some nebulizers for aerosol therapy,<sup>1,2</sup> in mass spectrometers as a means to reduce charging of polymer macroions generated by the electrospray ionization (ESI) technique,<sup>3,4</sup> and in the manufacture of nanoparticles by coalescence of oppositely charged nanodroplets followed by their drying.<sup>5,6</sup> The counterions used in these applications have been generated either by corona discharge<sup>7,8</sup> or by air ionization in contact with a radioactive isotope.<sup>9–11</sup> Both of these techniques generate a variety of ions, radicals, and hot atoms. Recently we proposed a new electrospray neutralization (ESN) technique in which highly charged aerosol particles and macromolecular ions were generated by electrospraying and then were neutralized with small counterions (e.g., ionized solvent molecules) also generated by electrospraying.<sup>12</sup> ESI as a method of producing counterions is believed to be less damaging to aerosolized biological molecules because it produces fewer hot atoms and reactive radicals than corona discharge and radioactive isotopes. Indeed, it was demonstrated that alkaline phosphatase retained 100% of its functional activity in the ESN-generated aerosol.<sup>12</sup> However, there is no guarantee that other enzymes and DNA molecules could be

turned into a nanoaerosol without damage, because the ESN technology involves high-energy processes potentially dangerous for biological macromolecules: (i) formation of multicharged ions in the ESI and (ii) the gas-phase neutralization process. Considering a protein ion with  $Z = 8e$  elementary charges and assuming that the neutralization occurs upon the direct contact of a small counterion with the surface of a macroion with a hen egg white lysozyme (HEWL) molecule radius,  $r_o = 1.7$  nm, we obtain for the impact energy  $U = Ze^2 / 4\pi\epsilon_0 r_o \sim 7$  eV (here,  $\epsilon_0$  is the vacuum dielectric constant), which is high enough to break a few chemical bonds. Do chemical bonds really break upon neutralization? How quickly is the impact energy dissipated? How does the hydration shell affect the neutralization process? These questions remain unanswered.

Attempts to retain protein structure and function in biological aerosols generated by the ESN process should also take into account the possible chemical reactions involved in the ESN process. Thus far, chemical reactions accompanying neutralization of ESI-generated macromolecular ions have been studied within quadrupole ion-trap mass spectrometers.<sup>13</sup> Multiple reactions involving proton transfer and other reactions were recently reviewed by Pitteri and McLuckey.<sup>14</sup> These

Received: January 12, 2012

Revised: April 30, 2012

Published: May 3, 2012

studies demonstrated that in the neutralization of multicharged positive ions with singly charged negative ions, transfer of protons dominates over reactions involving transfer of electrons, and therefore the chemical integrity of aerosolized biological molecules should not be compromised. Electron transfer was noted only in reactions involving ions of highly conjugated molecules.

Proteins and other hydrophilic biological molecules will readily bind water even in a relatively dry atmosphere, and the presence of water molecules on the protein surface is expected to greatly affect the outcome of the ESN process. The role of hydration in neutralization upon soft landing was studied in our earlier development of the electrospray deposition (ESD) technique.<sup>15</sup> We showed that the specific enzyme activity of alkaline phosphatase subjected to ESD was a function of air humidity, with the maximum retention of enzyme activity at a relative humidity of  $A = 20\text{--}40\%$ . While the decrease in the enzyme activity at  $A \sim 70\%$  is well-known and explained by the thermodynamic instability of solid protein samples under such conditions,<sup>16</sup> the drop in activity at  $A = 20\%$  was hard to explain.

This paper reports the first molecular dynamics (MD) simulations of gas-phase neutralization of multiply charged protein macroions with small counterions. It shows that hydration stabilizes the native structure of the protein macroion and protects protein molecules in collisions. Simulations show that collisions with a hydrated protein ion happen at larger distances from the protein surface and that the impact energy is mostly channeled to the solvent molecules, resulting in the energy rapidly dissipating among the numerous degrees of freedom of the bound water molecules. Thus, the water shell protects protein ions upon neutralization in the gas phase.

**Simulation Techniques.** The study was carried out using the MD program PUMA,<sup>17,18</sup> developed at the IMPB RAS by one of the authors (Balabaev). The system of Newton's equations was resolved in an all-atom force field, AMBER-99,<sup>19</sup> for all the protein and water atoms. It was found that correct predictions of the electrostatic stability of charged water droplets, corresponding to the Rayleigh limit, could be obtained only when no distance cutoff was imposed on the electrostatic forces.

The TIP3P model<sup>20</sup> was used for water molecules with the intermolecular bonds and angles not fixed, but limited with the appropriate potential functions. To maintain a constant temperature during system relaxation, a collisional thermostat was used as described in the literature.<sup>21,22</sup> Equations of atomic motions were integrated numerically using the velocity version of the Verlet algorithm<sup>23</sup> with time steps of 0.5 and 1 fs ( $10^{-15}$  s). The simulated system was enclosed in a sufficiently large sphere with an impermeable repulsive wall. The wall was represented by a short-distance purely repulsive potential for the interaction between atoms and the sphere. With the repulsive force operating at distances below 0.1 nm, the presence of such a wall did not affect the dynamics of the protein and water molecules and, at the same time, kept the water molecules within the sphere. Most simulations were made using the supercomputer JSCC RAS (<http://www.jsc.ru>).

To visualize the distribution of the collisional energy over the macroion and solvent molecules, we employed here a somewhat arbitrary "temperature" parameter for each atom in the system. This was estimated as the kinetic energy of each atom averaged over 1000 time steps, 0.5 fs each.

**Preparation of Relaxed Protein Macroions.** The major object for the MD simulations consisted of a positively charged HEWL molecule surrounded by a layer of water molecules containing both free and bound protons. The HEWL structure in solution was taken from the Protein Data Bank (a set 1GXV obtained by NMR) and used as the initial structure. The following procedure was used to prepare the sample for simulation. The protein macromolecule was first introduced into a water medium comprised of regularly spaced water molecules. Water molecules less than 0.3 nm and more than a certain distance,  $d_{\max}$ , from the closest protein atom were discarded. The value of  $d_{\max}$  was chosen to achieve a specified level of protein hydration. The thus prepared protein–water system was surrounded by a repulsive sphere with a diameter of 30 nm and was allowed to reach equilibrium under thermostat conditions at a temperature of 298 K.

A series of relaxed hydrated HEWL macroions (with the number of charges  $+8e$  and  $+18e$ ) was prepared with different numbers of water molecules, as listed in Table 1. HEWL with Z

**Table 1. Heating of HEWL Macroions Due to Collision with Different Counterions under Different Hydration Conditions**

charge of HEWL ion <sup>a</sup>	counterion <sup>a</sup>	$\Delta T^b$ , K (time from start <sup>c</sup> , ps)
$+8e(0)$	$\text{NO}_3^-(0)$	21(8.0); 23(15.2); 21(8.7); 23(8.4)
$+8e(300)$	$\text{NO}_3^-(0)$	9(12.2); 11(19.6); 9(8.7); 8(10.8)
$+8e(0)$	$\text{OH}^-(0)$	28(8.6); 25(6.5); 24(5.6); 22(5.4)
$+8e(0)$	$\text{OH}^-(10)$	22(17.9); 24(28.1); 21(22.3); 25(16.3)
$+8e(0)$	$\text{OH}^-(100)$	30(45.2); 32(117.6); 33(52.3); 32(44.0)
$+8e(300)$	$\text{OH}^-(10)$	8(19.8); 9(22.5); 10(17.2); 7(17.1)
$+8e(300)$	$\text{OH}^-(100)$	10(87.3); 12(60.2); 9(49.9); 11(49.6)
$+18e(300)$	$\text{OH}^-(0)$	16(4.4); 17(4.4); 16(3.4); 17(3.7)
$+18e(300)$	$\text{OH}^-(10)$	12(13.8); 13(14.9); 14(13.7); 14(11.5)

<sup>a</sup>The number of water molecules surrounding the macroion and the counterion is shown in parentheses. <sup>b</sup>Temperature raise in 50–200 ps after collision when the collision energy becomes distributed over the whole molecule and the temperature is stabilized. <sup>c</sup>Time from start to collision in picoseconds is shown in parentheses.

$= +18e$  bound charges corresponds to the maximal charge state reported in ESI mass spectrometry (ESI/MS) studies.<sup>24</sup> While  $+8e$  charges were positioned as provided by the 1GXV set, 10 additional bound protons in the latter HEWL macroion were localized on each of the Glu, Asp, and His residues, so that all the acidic residues were neutralized, and all the basic residues were charged as it is expected to happen in a proton-loaded microdroplet generated at a positive potential. A similar approach was taken by Reimann et al.<sup>25</sup>

It should be noted that ESI of the HEWL from water solution at a neutral pH generates macroions, among which those with  $Z = +8e$  are the most abundant. This charging state is also close to the limiting number of free charges on a water droplet the same size as the HEWL molecule. The latter estimate was made using the Rayleigh formula ( $Z_{\max}e$ )<sup>2</sup> =  $64\pi^2\sigma\epsilon_0R^3$  (here  $\sigma$  is the surface tension of water). For a water nanodroplet, with an average radius comparable to the average radius of the HEWL globule ( $R = 1.8$  nm), this formula gives  $Z_{\max} = +9e$ . This relationship between the charging state and the Rayleigh limit provides a basis for the Dole's mechanism of protein ion formation in the ESI process in the form of dry residues.<sup>26</sup> In some simulations, 1–7 free protons were

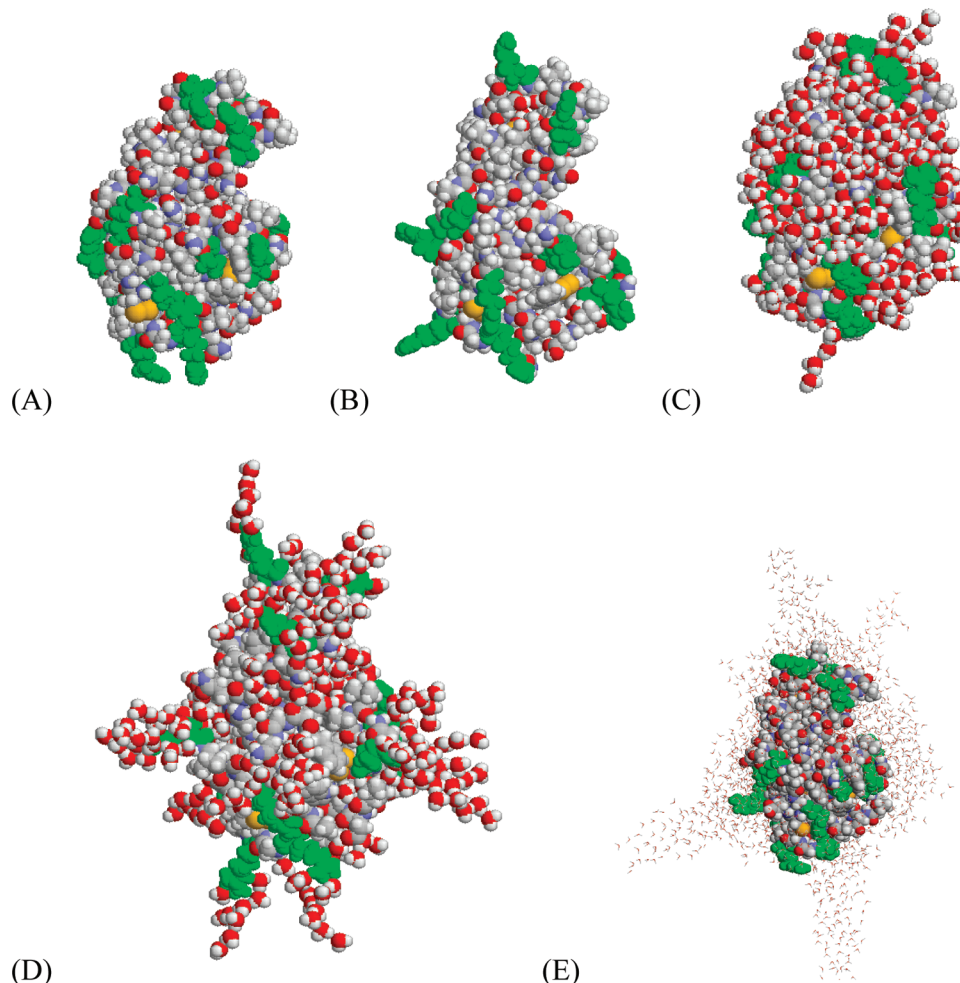


**Figure 1.** Structures of the relaxed HEWL macroions with different charges at different hydration levels in comparison with the native structure. (A) NMR structure of HEWL in solution. (B) Dry HEWL ion with  $Z = +18e$ . (C) A hydrated HEWL ion with 300 water molecules and  $Z = +8e$ . (D) A hydrated HEWL ion with 300 water molecules and  $Z = +18e$ . (E) Water spines on a highly hydrated HEWL ion with  $Z = +18e$  and 1500 water molecules. Arg, Lys, and His residues are colored green. Unlike the rest of the panels, where the water molecules are shown as space-filling models, the water molecules in structure E are depicted using a wireframe model to make the protein surface visible. Atoms of carbon, oxygen, nitrogen, hydrogen and sulfur are depicted as gray, red, blue, white, and yellow spheres, respectively.

introduced into the system to see how liberation of charges modifies the behavior of the hydrated macroion and how free protons leave the macroion.

Both the HEWL ions with  $Z = +8e$  and those with  $Z = +18e$  were allowed to relax in contact with 300 and 1500 water molecules for a total time of 1 ns. The former number roughly corresponds to a hydration shell around the protein globule<sup>27</sup> and is close to the hydration level of lysozyme molecules in crystalline and amorphous solid samples.<sup>28</sup> The latter, much higher, hydration level was chosen to see how an excess of water affects the water shell structure around the charged protein macroion.

**Simulation of Counterion Impact in the Gas-Phase Neutralization Process.** In simulations of the neutralization process, a counterion was placed within the same sphere at a distance of 10 nm from the center of the protein macroion. The collision process was simulated in the thermally isolated system with the thermostat switched off.

Simulations of the collision event were performed for two small anions: (i) the smallest negative ion observed in the corona discharge at a negative potential, hydroxide anion,  $\text{OH}^-$ , and the most abundant negative ion observed in the negative

corona,<sup>29</sup>  $\text{NO}_3^-$  ion. These ions were taken as both naked and covered with a layer of water molecules. Although most stable water clusters around an  $\text{OH}^-$  ion contain only 3–4 water molecules according to the MS data,<sup>30</sup> in our simulations we used arbitrary 10 and 100 water molecules. The latter number is supported by recently published MS data showing that, in the absence of severe desolvation, even at the relatively low humidity of  $A = 40\%$ , corona-generated negative ions were surrounded by up to 200 water molecules.<sup>31</sup> The choice of the lower hydration level of 10 water molecules was based on our observation that in an MD simulation of the electrostatic decay of highly charged hydrated HEWL molecules, protons left the charged droplet surrounded by 10–15 water molecules. Recent simulations of Ahadi and Konnerman<sup>32</sup> also demonstrated that  $\text{NH}_4^+$  ions that were evaporated from a charged water nanodroplet carried away 10–20 solvent molecules.

To understand the role of water in the energy dissipation, we also simulated events that are hard to achieve experimentally: the collision of dehydrated hydroxyls with hydrated HEWL ions, and that of hydrated hydroxyl anions with dehydrated HEWL macroions. The dynamics of the distribution of the impact energy was visualized by averaging the kinetic energy of

each atom in the system with a time interval of 0.5 fs. Averaging was performed for 1000 such steps, and the equivalent “temperature” was calculated for each atom. MD simulations were continued for 1 ns after collision. This time was sufficient for energy distribution over all the globule as judged by the total kinetic energy (temperature) reaching its steady level so that further relaxation resulted in less than 10% changes of this level.

The HEWL structures were analyzed for changes in the secondary structural elements. These were evaluated using the YASARA program.<sup>33</sup> We found that averaging the effects of the impact in terms of changes in the secondary structural elements made little sense because the effects of the impact varied dramatically depending on the collision location. Thus, the collision of a dry OH<sup>-</sup> ion with Arg-114 on the surface of +8e charged HEWL resulted in a decreased fraction of residues involved in the  $\alpha$ -helices, from 33.3% inherent to the native X-ray structure to a notably lower value of 20.9%, while a similar collision with Arg-73 changed the percentage only to 27.9%.

## RESULTS AND DISCUSSION

**Structure of Charged HEWL as a Function of Charge and Hydration.** Our simulations showed that a moderately charged HEWL molecule with  $Z = +8e$  substantially retains its native structure in the gas phase for at least 1–2 ns, even if completely dehydrated. The addition of 300 water molecules did not result in notable structural changes as can be seen from a comparison of structures A and C in Figure 1. As expected, water clusters predominantly coated polar and charged areas. These water-coated areas increased with increases in the total number of available water molecules until the whole protein surface became coated with a water layer at the hydration level of  $\sim 1000$  water molecules per HEWL molecule. These features of water distribution around the charged HEWL globule are in good accord with previous simulations of the hydrated HEWL macroion coated with a water monolayer,<sup>34</sup> which demonstrated that the hydrated molecule with +8e charges maintained its native structure and remained stable up to 425 K. Similar conclusions regarding the importance of solvent molecules to the stability of highly charged cytochrome C and ubiquitin macroions were made in the MD simulations made by Breukera and McLafferty.<sup>35</sup>

This good agreement justifies our choice of the AMBER force field parameters that were designed for simulations in the presence of solvent by taking into consideration a certain dependence of bond polarization on the presence of solvent molecules. Although it is known that partial charges of the surface residues on a dry globule differ from those in solution, the presence of a hydration layer on the gas-phase macroion in most practical cases justifies the choice of a solution-oriented force field set in our simulations. Simulations of a completely dry protein macroion were only made to evaluate the role of hydration in the dissipation of the impact energy, where slight solvent-dependent variations in the force field parameters do not change the process.

Unlike a moderately charged dry HEWL macroion, the one with  $Z = +18e$  charges bound to its surface displayed notable changes in the overall three-dimensional structure. Comparison of structures A and B in Figure 1 clearly shows two types of structural changes due to supercharging. First, the overall shape becomes more extended due to the domains’ motion. Second, the charged side chains of the Asp and Glu residues detach from the globular surface, producing the “hairy” protein

structure illustrated in Figure 1B. The latter changes decrease the electrostatic energy at the expense of breaking the hydrogen and other bonds that held the side chains attached to the globular surface in the initial HEWL structure. The presence of water notably inhibits the structural changes resulting from such supercharging. A comparison of structures A, C, and E in Figure 1 shows that the structure of the supercharged HEWL in the presence of 1500 water molecules is closer to that of a native HEWL molecule and gas-phase macroion with  $Z = +8e$  charges than to the dry supercharged HEWL depicted in Figure 1B.

In the presence of water, electrostatic repulsion energy works not to perturb protein structure but rather to change the water structure around the protein ion, thereby decreasing the electrostatic energy. As seen in Figure 1D, water molecules on the surface of the supercharged HEWL form chains of oriented water molecules in which water dipoles are directed with positive poles away from the protein surface. From the standpoint of electrostatic interactions, these chains of oriented dipoles move the positive charges away from the protein surface, increasing the distances between these virtual charges and decreasing the overall electrostatic repulsion energy. When the number of water molecules was increased to 1500, the water molecules formed spectacular protrusions or spines, seen in Figure 1E. Although water molecules in the spines are subjected to intensive thermal motion, as illustrated in the movies provided in the Supporting Information, they still keep the same predominant dipole orientation of negative poles directed to the positive charges on the protein surface.

We should emphasize that the description of the water’s behavior at different charging levels corresponds well to the macroscopic model of a charged water droplet. The Rayleigh limit for a water nanodroplet of a size similar to that of the HEWL molecule hydrated with 300 H<sub>2</sub>O is estimated as  $Z_{\max} = +9e$ . Therefore, at  $Z = +8e$  water molecules form smooth islands on the protein surface with occasional protrusions, as seen in Figure 1C. When the number of bound charges exceeds the Rayleigh limit (Figure 1D,E), the hydration layer becomes rough, showing “spines”, which have been described by several authors.<sup>36,37</sup> The spines were formed in  $\sim 50$  ps over the charged residues and/or constellations of charges. Although water molecules were seen to change position inside the spines and between the spines, the locations of the spines were invariant. When the number of charges was high ( $Z = +18e$ ) at a relatively low hydration (300 water molecules per HEWL molecule), practically all of the water molecules were in the spines. An important difference between the behavior of a charged droplet and that of a charged macroion originates from the fact that the charges are immobilized on the macroion structure and cannot leave the droplet on reaching the Rayleigh limit. As Consta showed for a positively charged highly hydrated polyhistidine macroion,<sup>36</sup> water does not leave the overcharged droplet but forms spines consisting of arrays of oriented water dipoles growing from His charges. Such arrays of oriented dipoles effectively transfer charges from His residues to the tips of spines, thus minimizing the electrostatic repulsion energy. We see the same picture in Figure 1D,E.

Free protons were occasionally seen to leave the largest spines together with 10–15 water molecules, in accordance with the previous simulations.<sup>37</sup> It is worth noting that the free protons did not tend to occupy the tips of the water spines, although that would minimize the energy of the electrostatic repulsion. We speculate that moving to the spine tip would

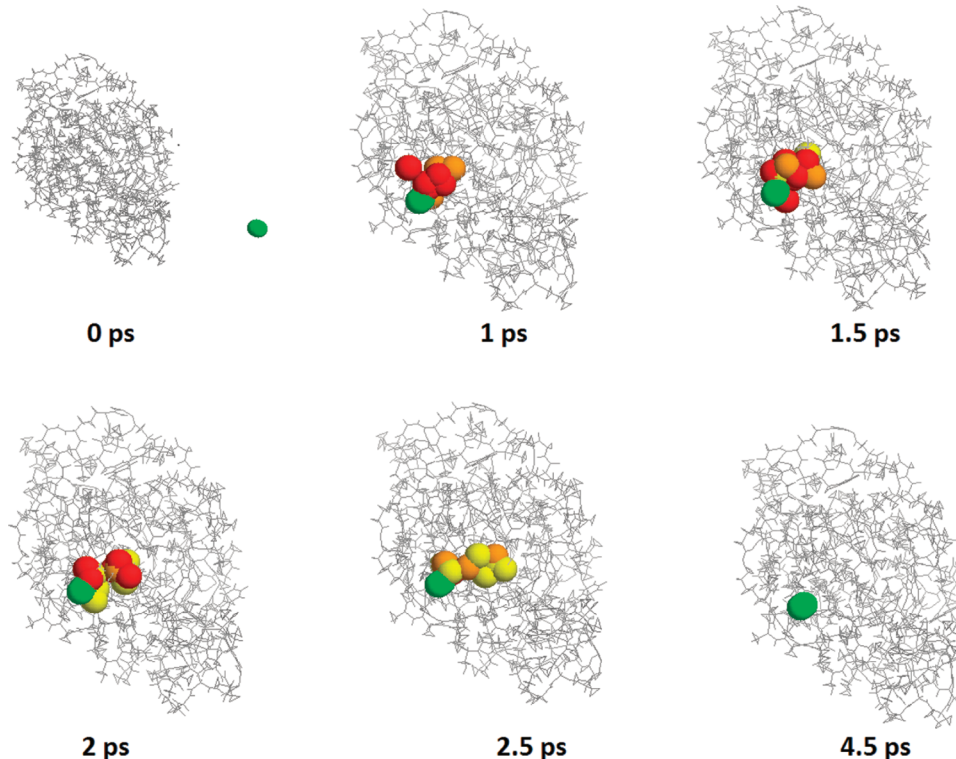


**Figure 2.** Dynamics of heat distribution in a dehydrated HEWL macroion with  $Z = +8e$  as a result of impact with desolvated hydroxide anion (represented by a green ball). Atom color reflects the instant local temperature: red indicates atoms with an effective temperature exceeding 1000 K, orange indicates those in the temperature range of 900–1000 K, and yellow indicates the range of 800–900 K. Numbers under each panel denote the time passed after the counterion touches the HEWL surface. The image at 0 ps is on a smaller scale to make room for the hydroxyl ion.

result in an unfavorable decrease in proton hydration. This explanation is supported by recent simulations of the distribution of ions in a charged water droplet by Ahadii and Konermann.<sup>38</sup> They showed that the ions do not occupy the droplet surface as expected from a purely electrostatic argument; instead, the ions are distributed within a concentric layer inside the charged droplet. Such dipping into the droplet does not increase the repulsion energy because the charges are efficiently transferred to the droplet surface via arrays of oriented water dipoles.

**Collision of a Small Counterion with a Hydrated Multicharged HEWL Ion.** To evaluate the role of different factors in collision events, we tested different combinations of dry and hydrated HEWL targets as well as solvent-free and hydrated counterions. These combinations are listed in Table 1, which also presents the overall increase in temperature resulting from each simulated collision and the time needed for the counterion to reach the protein surface starting at the same distance from the center of the HEWL globule.

We chose two hydration levels for  $\text{OH}^-$  ions: 10 and 100 water molecules. This choice was based on MS studies of corona products that showed that in the absence of the conventional strong dehydration induced by passage through a heated capillary, all of the corona products are heavily hydrated, even at low humidity. Up to 300 water molecules were reported to coat small corona-generated ions.<sup>31,39</sup> This water shell was surprisingly stable: it survived for up to 70 microseconds in high vacuum. Similarly, Sekimoto and Takayama<sup>30</sup> found that the mass spectrum of corona products generated at room temperature in ambient air with a relative humidity of 25% contained water clusters,  $\text{OH}^-(\text{H}_2\text{O})_n$  with  $n = 1–13$ .

Although at large distances a negative counterion is attracted to a protein macroion by the overall charge of the protein ion,  $+Ze$ , at a closer distance the local electric field prevails, and the counterion usually lands on the positive charge or on a constellation of closely placed positive residues on the dry protein ion. In the presence of a hydration shell, the collision started with contact of the counterion with the water molecules.

Table 1 shows that the time needed to reach the protein surface varied substantially depending on whether the counterion was desolvated or solvated. In the latter case, the time was notably longer because the larger mass of solvated ion resulted in lower velocity at the same kinetic energy. Although counterions fell from the same distance with respect to the globule center, we observed substantial variations of the landing time in a series of simulations with identical ions. We speculate that small variations in the electric field due to the dipole field as well as variations in the direction of the initial ion impulse,  $(3mkT)^{1/2}$ , are responsible for the observed scatter in the approaching time. The direction of initial impulse determined the landing location as well: with the initial impulse directed perpendicularly to the vector connecting the centers of the counterion and protein macroion, orbiting around the protein ion was observed in some simulations. Movies provided in the Supporting Materials illustrate the dynamics of counterions approaching a HEWL ion and collision events under different hydration and charging conditions.

Collision of a bare hydroxide  $\text{OH}^-$  anion with a dry HEWL macrocation resulted in an instant increase in temperature among a few atoms in close proximity to the impact location. Illustrations of this local temperature increase in the impact area are presented in Figure 2, and the time dependence of the

number of heated protein and water atoms is shown in Figure 3. We see that, although the local temperature increase was

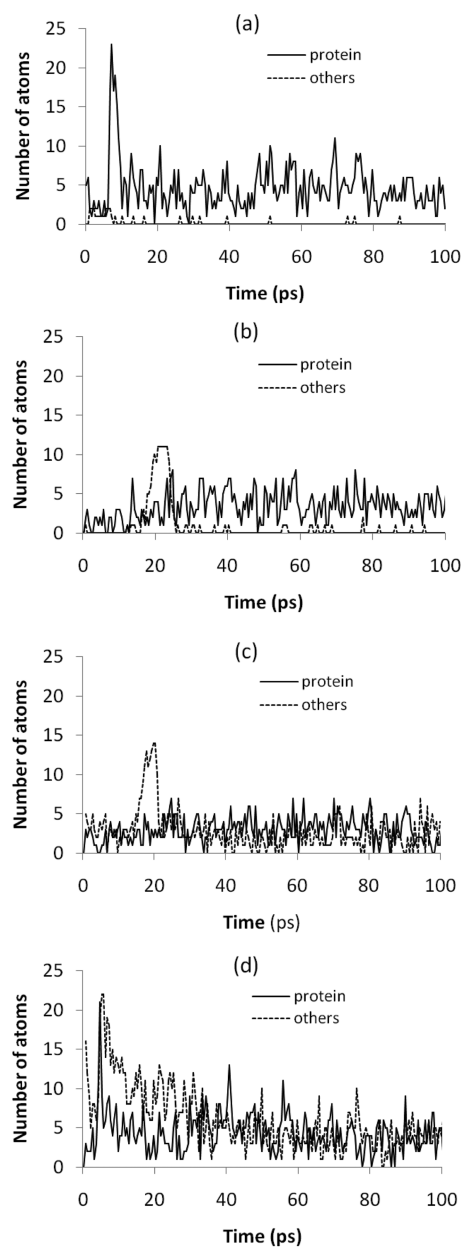


**Figure 3.** Changes in the number of energized protein and water atoms in the HEWL macroion after collision with a hydroxyl ion. Ordinates denote the number of atoms with an effective instant temperature exceeding 700 K. (a) Number of hot atoms in a dry HEWL macroion after impact with a bare  $\text{OH}^-$  ion. (b) Number of hot atoms in a dry HEWL macroion after impact with an  $\text{OH}^-$  ion coated with 10 water molecules. (c) Number of hot atoms in a hydrated HEWL ion (300 water molecules) after collision with the hydrated  $\text{OH}^-(10\text{H}_2\text{O})$ . (d) Number of hot atoms after collision of a desolvated hydroxyl ion with a supercharged hydrated HEWL ion with  $Z = +18e$  (300  $\text{H}_2\text{O}$ ). Zero time indicates the start of collision simulation, which includes approach time.

high ( $>1000$  K), it persisted for only 1–5 ps in the impact area before the impact energy spread over the entire protein structure.

Collisions in the presence of hydrated water were modeled under three different conditions: (i) only the protein ion is

hydrated, (ii) only the counterion is hydrated, and (iii) both macroion and counterion are hydrated. Although some situations seem to be out of reach of experimentation (such as having only one of the ions hydrated), comparing the simulation results allows us to understand the role of water in dissipating the collision energy. As we see in a series of curves in Figure 3, in all the cases studied, the presence of water in the collision area resulted in a notably lower number of hot protein atoms (with  $T > 700$  K) irrespective of whether the water molecules belonged to the protein water shell or were brought with the counterion. Moreover, this local heating was now mostly applied to the water molecules in the impact area, while the protein atoms were subjected to much lower heating.

Collision with the dry HEWL macroion resulted in overheating of 22 protein atoms, which took about 5 ps to disappear. Collision with a hydrated macroion with  $Z = +8e$  did not show any pulse of overheated protein atoms above the normal fluctuation level, as we see in Figure 3b,c. Only when the number of charges was increased to 18 were overheated protein atoms seen again. While the protein atoms lost their excessive energy almost as quickly as in dry HEWL (compare panels a and d in Figure 3), the overheated water atoms kept their energy 5–10 times longer than the HEWL atoms. We attribute this difference in the speed of energy relaxation to the different mechanisms of energy exchange in these two systems.

From the data presented in Figure 3 and Table 2, it is evident that hydration of the  $\text{OH}^-$  anion by 10 water molecules notably

**Table 2. Average Number of Hot and Superhot Atoms Generated in the HEWL Macroion upon Collisions with Different Ions at Different Hydrations of Protein and Colliding Ions**

protein charge (hydration) <sup>a</sup>	colliding counterion (hydration) <sup>a</sup>	number of hot atoms <sup>b</sup>	number of superhot atoms <sup>c</sup>
+8e(0)	$\text{NO}_3^-(0)$	$12 \pm 3$	$3 \pm 2$
+8e(0)	$\text{OH}^-(0)$	$20 \pm 3$	$7 \pm 2$
+8e(0)	$\text{OH}^-(10)$	$10 \pm 1$	0
+8e(300)	$\text{NO}_3^-(0)$	$10 \pm 2$	0
+8e(300)	$\text{OH}^-(10)$	$8 \pm 1$	0
+18e(300)	$\text{OH}^-(0)$	$15 \pm 4$	$4 \pm 2$
+18e(300)	$\text{OH}^-(10)$	$9 \pm 1$	0

<sup>a</sup>Number of water molecules on each ion is indicated in parentheses.

<sup>b</sup>Average of four independent MD simulations of collisions. The average number of atoms with  $T > 700$  K is presented for each set of collision conditions. <sup>c</sup>Average of four independent MD simulations of collisions. The average number of atoms with  $T > 1000$  K is presented for each set of collision conditions.

changed the collision outcome: the number of instant hot atoms was half that of the collision of a dry  $\text{OH}^-$  ion. Moreover, those hot atoms mostly belonged to water molecules, as is evident in Figure 3b. Even in the presence of 300 water molecules on the supercharged HEWL macroion, hydration of the colliding  $\text{OH}^-$  with only 10  $\text{H}_2\text{O}$  notably reduced the number of hot atoms, as we see in Table 2. Yet another consequence of the counterion hydration seen in Table 2 is the absence of superhot atoms with  $T > 1000$  K on the supercharged hydrated HEWL when the hydroxide counterion was also hydrated.

It is also evident from Table 2 that despite the equal total energy of the impact with  $\text{OH}^-$  and  $\text{NO}_3^-$  anions, the  $\text{OH}^-$  anions produced a notably larger number of hot atoms. We

attribute this difference to the smaller number of freedom degrees in the hydroxide ion: 6 and 12 for the di- and four-atomic anions, respectively. With a larger fraction of the collision energy spent to pump up the internal freedom degrees in the colliding  $\text{NO}_3^-$  ion, less energy was left to heat the protein atoms.

To investigate how the simulated temperature increase corresponds to the real properties of the HEWL molecule, we compared the calculated impact-induced temperature increase in the dry HEWL macroion with the expected temperature increase estimated from the known experimental heat capacity of the native protein molecules. As is shown in Table 1, a single collision increases the temperature of a dry HEWL molecule by  $\Delta T = 20\text{--}25\text{ K}$ . Considering that the heat capacity of solid protein material is mostly due to intramolecular vibrations and has a value<sup>40</sup> of  $C_p = 1.20\text{ J/K}$  per 1 Da at 298 K, heating by the average 24 K increases the HEWL enthalpy by an estimated  $\Delta H = MC_p\Delta T = 420\text{ kJ/mol}$  (here  $M = 14.5\text{ kg}$  is the molar mass of the HEWL molecule). Although part of the collision energy might have been spent on changes in the interatomic distances in the adiabatic process, the difference between  $C_p$  and  $C_v$  in proteins is less than 5% according to one study;<sup>41</sup> therefore, the increase in internal energy occurs mostly due to the enthalpy change, which can be estimated as  $\Delta U = \Delta T M C_v \approx \Delta H = MC_p\Delta T$ . The estimated increase in the internal energy should be compared with the collision energy. The collision energy may be estimated in two ways. First, a simple electrostatic model assumes that all +8e charges are placed in the center of a sphere with radius  $r_o = 1.7\text{ nm}$  and that the neutralizing counterion starts accelerating at a distance of  $r_m = 10\text{ nm}$  from the HEWL center and increases its kinetic energy until physical contact with the HEWL surface is reached. It finds that the impact energy  $\Delta U = (Ze^2/4\pi\epsilon_0)(1/r_o - 1/r_m) = 550\text{ kJ/mol}$ , in very good agreement with the above estimate for changes in the internal energy from heat capacity. Yet another, more precise, estimation of the collision energy may be obtained directly by averaging the kinetic energy of a counterion before its collision with the macroion surface. In a series of these simulations, with the HEWL ion having  $Z = +8e$  charges, the  $\text{OH}^-$  ion acquired an energy of  $450 \pm 80\text{ kJ/mol}$ . This energy almost exactly matches the collision-induced increase in the internal HEWL energy by 420 kJ/mol, meaning that all the collision energy is transformed into heat.

Table 1 shows that in the presence of 300 water molecules on a +8e charged HEWL ion, the impact-induced temperature rises by only  $\sim 14\text{ K}$  instead of 24 K on the dry HEWL ion. This decrease in the temperature jump is well-explained by the increased heat capacity of the hydrated macroion. Assuming that the heat capacity of water in the hydration layer is similar to that of the bulk water,  $C_{pw} = 4\text{ J/g K}$ , we estimated the expected temperature increase to be  $\Delta T = \Delta H/(MC_p + m_w C_{pw})$ . Substituting for  $\Delta H$  the average collision energy ( $450 \pm 80\text{ kJ/mol}$ ), we obtain  $\Delta T = 12.3 \pm 2.2\text{ K}$ , which well suits the observed temperature increase.

It is interesting to note in the data presented in Table 1 that when 100 more water molecules were brought with the counterion to the HEWL ion already hydrated with 300 water molecules, no further decrease in the temperature jump was observed. We explain this difference between the water molecules that were already present on the protein surface and the newly arrived molecules by the following. Unlike the former, which were already bound to the protein surface, the latter establish bonds with the polar groups on the protein

surface after collision. The heat generated in the hydration process conceals a decrease in the overall temperature due to heat capacity of the water molecules brought by the counterion.

As can be seen from Table 2, superhot protein atoms appeared only in the collisions when both the HEWL ion with +8e charges and the counterions,  $\text{OH}^-$  and  $\text{NO}_3^-$ , were dehydrated, indicating that water molecules at the collision site effectively absorb the collision energy. However, when the collision energy increased in the case of the HEWL macroion with  $Z = +18e$ , overheated protein atoms with  $T > 1000\text{ K}$  appeared again at the collision site, even when the protein ion was hydrated (300  $\text{H}_2\text{O}$ ). In these cases, dry hydroxyls landed on the water-free area on the HEWL surface between the water spines. A visual depiction of local heating after collision of dry HEWL and bare hydroxide ion is available in the Supporting Information.

Figure 4 demonstrates changes in the temperature and in the fraction of residues involved in the  $\alpha$ -helical structures in a HEWL ion subjected to a series of six consecutive collisions, which raised the HEWL temperature by 87 K for the dry protein ion and by 57 K for the hydrated one. Notable structural perturbations accompanied the collisions with the dehydrated protein ion, while the secondary structure of the hydrated HEWL endured this bombardment. We therefore demonstrated that the hydrated HEWL macroion is notably more stable than the dry one: even the summation of a few collisions without energy exchange with the environment did not result in substantial conformational changes, i.e., the hydration layer effectively protected the protein structure in multiple collisions. Under real conditions in the ESN process, the protein ion has enough time to cool down between collisions, as simple estimates show. In the Appendix, we present rough estimates for the average time between collisions as well as estimates for the cooling time due to collisions with air molecules and due to radiative energy loss. Although admittedly crude, these estimates show that under typical experimental ESN conditions where the neutralization events happen with an average interval of  $\sim 1\text{ }\mu\text{s}$  on each macroion, the collision energy will be completely exchanged with the surrounding gas between the collisions so that summation of several consecutive collisions can be considered highly improbable. Therefore, conclusions about the structural and temperature outcomes of a single collision can be extended to the whole ESN process.

We have demonstrated by these simulations that the hydration water shell should provide substantial protection against damage to fragile protein and other biological macromolecules aerosolized by the ESN process. Since most biological molecules are hydrophilic by nature, they will necessarily be covered with a protective layer of water molecules under ambient conditions. This explains why alkaline phosphatase retained nearly 100% of its specific enzyme activity when electrosprayed at moderate humidity but showed a marked decrease in activity when deposited in air dried over silica gel.<sup>15</sup> In the latter case, the enzyme molecules were deprived of the protective water shell upon collision with the metal substrate. Similarly, the structure and functional activity of many proteins were retained when ESD was performed in conditions that were not completely dry.<sup>15,42</sup>

What are the chances that gas phase neutralization is accompanied by fragmentation of biological molecules? Our simulations show that bare  $\text{OH}^-$  ion before collision with a HEWL macroion having  $Z = +8e$  charges acquires an energy of

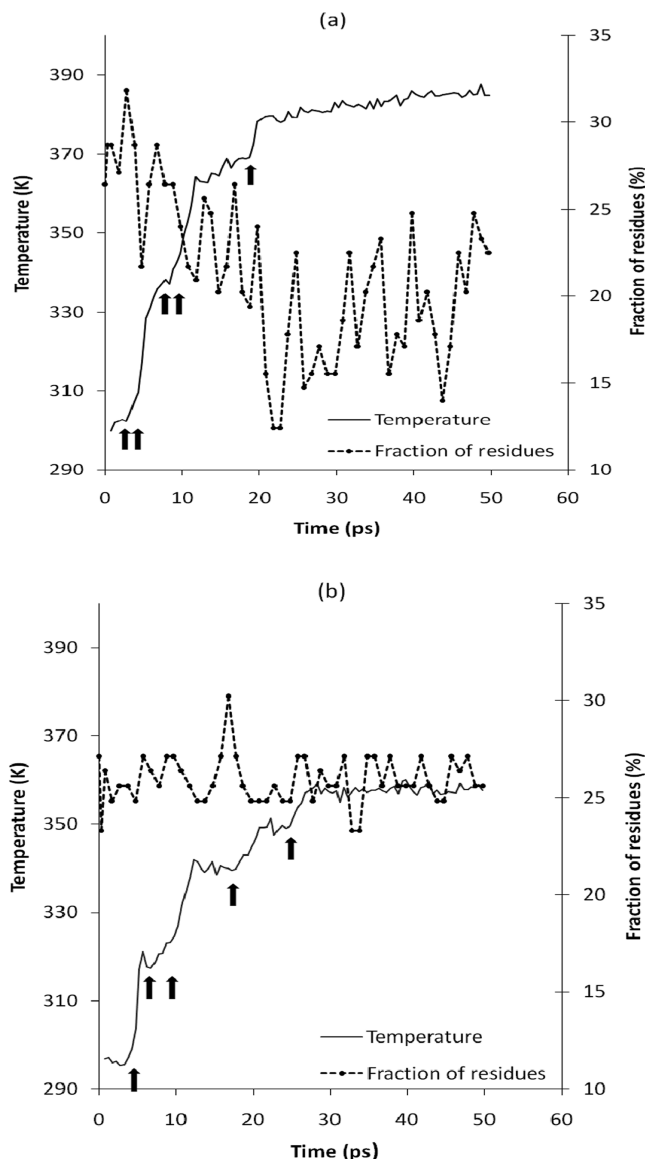


**Figure 4.** Changes in the temperature and secondary structural elements as a result of the summation of a series of multiple collisions with  $\text{OH}^-$  ion. (a) Dry HEWL molecule having charge  $+8e$ . (b) Similarly charged HEWL molecule with 300 water molecules. Right ordinates represent the fraction of residues that form the helical structures. Left ordinates show average temperature. Arrows indicate collision events.

$450 \pm 80 \text{ kJ/mol}$ , or  $4.7 \pm 0.8 \text{ eV}$ . Considering that this energy is initially distributed among 3–10 atoms during the contact between the counterion and atoms on the protein surface and that the activation energy for cleavage of the amide and C–C bonds is  $\sim 0.5\text{--}1.2 \text{ eV}$ ,<sup>43</sup> we can conclude that collision of a dehydrated  $\text{OH}^-$  ion provides enough energy to fragment a peptide bond. Moreover, we must take into account that the electrospray-generated counterions are born hot due to repulsion from the charged mother nanodroplets; they acquire<sup>44</sup> initial kinetic energy corresponding to a temperature of  $600\text{--}1000 \text{ K}$ . Although this energy excess will be lost in a few collisions with the air molecules within  $\sim 10 \text{ ps}$ , these hot counterions might also contribute to the fragmentation of protein ions in the ESN process under dry conditions. Even though such fragmentation can take place to some extent, our

simulations clearly demonstrate that the presence of hydration water on the protein surface should dramatically reduce the fragmentation probability.

## CONCLUSIONS

To the best of our knowledge, this is the first report on simulating the neutralization of highly charged hydrated protein macroions in air under ambient conditions. Using MD simulations, we demonstrated a substantial protective effect of protein hydration, which channels the collision energy predominantly to the water molecules. The collision of a single hydroxide ion with a dehydrated positively charged lysozyme ion results in high local heating of a few protein atoms by as much as  $\sim 1000 \text{ K}$ . The energy is then quickly dissipated, raising the average temperature of the whole HEWL molecule by  $\sim 20 \text{ K}$ . Given the collision energy and the high local temperature at the collision site, it is possible that some chemical changes might accompany the gas-phase neutralization of dry protein macroions. Neutralization in the presence of a water shell around a protein ion is expected to cause much less damage for several reasons. First, the collision occurs not with the protein atoms but with the bound water molecules. Second, the impact energy is released to the water molecules and distributed over a large number of their degrees of freedom, resulting in a relatively small temperature increase and in smaller mechanical forces being applied to the protein atoms. Third, the collision-induced temperature increase averaged over the whole molecule is also reduced in the hydrated macroion due to the larger overall heat capacity of the hydrated protein ion. Thus, maintaining a certain hydration level on the protein gas-phase ions and on drug nanoparticles is required during manufacturing of biological and biologically active nanoaerosols by the ESN technique. On the other hand, when the aim is gas-phase fragmentation or modification of protein molecules, dehydration of protein macroions should be performed before the neutralization to avoid the damping effect of water molecules in the neutralization collisions.

## APPENDIX

### A1. Estimation of Time between Neutralization Events in the ESN Process under Ambient Conditions

A typical concentration of counterions generated in ESI can be estimated as follows: A jet of ESI products at a distance of  $l = 1 \text{ cm}$  has a cross-section of  $S = 1 \text{ cm}^2$  and a rate of  $v \sim 10 \text{ m/sec}$ .<sup>45,46</sup> Assuming that all the charges turn into hydroxyls, we obtain that at a typical current of  $I = 100 \text{ nA}$ , the concentration of counterions in the jet should not exceed  $C_h = I/e\pi Sl = 0.6 \times 10^9 \text{ ions/cm}^3$ . Thus, in the space where neutralization takes place, the average distance between the counterions should be  $a = (1/C_h)^{1/3} = 12 \mu\text{m}$ . To reach a protein ion by pure diffusion in the absence of electrostatic attraction, a counterion should pass through half of this distance, which would require a time of  $\tau_d = a^2/8D = 0.8 \mu\text{s}$ . Here we took the diffusion coefficient for  $\text{OH}^-$  ion<sup>47</sup> at a normal air pressure to be  $D = 0.22 \text{ cm}^2/\text{sec}$ .

How does the presence of charges on the protein macroion affect this estimate? Taking the known mobility of light negative ions<sup>29</sup> such as  $\text{OH}^-$  to be  $\chi = 2 \text{ cm}^2/\text{V sec}$ , we obtain that at a distance of  $a/2 = 6 \mu\text{m}$ , the velocity of the  $\text{OH}^-$  ion will be  $V_{\text{OH}} \sim \chi Ze/\pi\epsilon\epsilon_0 a^2$ , and the time to reach the HEWL macroion will be  $\tau_e \sim a/2V_{\text{OH}} = \pi\epsilon\epsilon_0 a^3/2\chi Ze$ . For the HEWL ion with the highest charge  $Z = +18e$ , we estimate that the average time needed for  $\text{OH}^-$  ion to reach the macroion when only electrostatic force controls the motion is  $\tau_e \sim 40 \mu\text{s}$ . Its

comparison with  $\tau_d = 0.8 \mu\text{s}$  shows that the attraction of charges does not accelerate neutralization at a typical counterion density in our ESN process, and that the neutralization kinetics of multi-charged protein ions are controlled mostly by the thermal diffusion of small counterions.

#### A2. Estimation of Cooling Time for a Protein Ion under Normal Air Pressure

There are two channels for dissipation of the excess energy from aerosolized protein ions: (i) heat exchange due to collisions with the air molecules and (ii) radiative energy loss. Let us estimate the times needed to cool down a HEWL molecule heated by a collision with a counterion by both mechanisms.

Considering the HEWL molecule to be a ball with radius of  $R = 1.7 \text{ nm}$ , and using the kinetic theory of gases, we obtain for the number of air molecules colliding with the protein in a time unit:

$$N = (2\pi R^2/3)N_L\langle v \rangle \quad (1A)$$

where  $N_L = 2.7 \times 10^{19} \text{ cm}^{-3}$  is the Loschmidt constant, and  $\langle v \rangle \sim 300 \text{ m/sec}$  is the average velocity of thermal motion of air molecules at room temperature. Thus, an air molecule collides with the HEWL ion every  $\tau_a = 1/N = 20.5 \text{ ps}$ . Assuming that the temperature of the protein ion will be approximately halved when the number of collisions is equal to the number of atoms in the protein molecule, we obtain for the characteristic collision-based cooling time  $\tau_c \sim 2000\tau_a = 40 \text{ ns}$ .

Radiative energy loss may be estimated from the Stefan–Boltzmann law for the total energy radiated per unit surface area of a black body per unit time,  $E_n = \sigma T^4$ , where  $\sigma = 5.67 \times 10^{-12} \text{ W cm}^{-2} \text{ K}^{-4}$  is the constant, and  $T$  is the absolute temperature. Thus, the energy excess  $\Delta G = C_p m \Delta T$  due to heating by  $\Delta T = 20 \text{ K}$  will be lost due to radiation in a time scale of

$$\tau_r \sim C_p m \Delta T / 4\pi R^2 \sigma T^4 \quad (2A)$$

Substituting into eq 2A protein heat capacity  $C_p = 1.2 \text{ kJ/kg grad}$ ,<sup>40</sup> protein mass  $m = 2.4 \times 10^{-20} \text{ g}$ ,  $\Delta T = 24$ , and  $T = 300 \text{ K}$ , we obtain  $\tau_r \sim 40 \mu\text{s}$ . Because  $\tau_c \ll \tau_r$ , collisions with the air molecules should provide the major way for dissipation of the excessive protein energy gained from the high-energy impact. Because  $\tau_c \sim 40 \text{ ns}$  is at least an order of magnitude smaller than the average time between the collisions estimated in Appendix A1, we conclude that the protein macroion has enough time to dissipate the excessive thermal energy between the neutralization events.

#### ASSOCIATED CONTENT

##### Supporting Information

Movie 1: Relaxation of droplet containing multicharged (+18e) HEWL and 300 water molecules. Almost all the water molecules are distributed in spines. Movie 2: Collision of hydrated (300 H<sub>2</sub>O) HEWL Z = +8e and a bare NO<sub>3</sub><sup>-</sup> ion. Scattering of water molecules from the collision site is visible. OH<sup>-</sup> ion is colored red. Movie 3: Collision of dry HEWL and a bare hydroxide ion. Atoms are painted according to their average kinetic energy; local “heating” near the place of impact is visible. Atoms colored in blue have a temperature  $T < 700 \text{ K}$ , while those colored in red have  $T > 900 \text{ K}$ . This material is available free of charge via the Internet at <http://pubs.acs.org>. This material is available free of charge via the Internet at <http://pubs.acs.org>.

#### AUTHOR INFORMATION

##### Corresponding Author

\*Address: Institute of Theoretical and Experimental Biophysics, Russian Academy of Sciences, Pushchino, Moscow Region, Russia 142290. E-mail: vmorozov@gmu.edu; Fax: 7-496-733-0553.

##### Notes

The authors declare no competing financial interest.

#### ACKNOWLEDGMENTS

The authors express their gratitude to the Joint Supercomputing Center of the Russian Academy of Sciences, where most of the calculations were made. The authors acknowledge funding from HDTRA (Grant # HDTRA1-09-14-FRCWMD-BAA). I.L.K. thanks the Skolkovo UMNIK fund for support. Fruitful discussions with Drs. Yuri Shlyapnikov, Elena Shlyapnikova, and Andrew Mikheev as well as the technical help of Ilya Likhachov are gratefully acknowledged. The authors also acknowledge the substantial contribution of Dr. Tamara Morozova to the preparation of the manuscript and the assistance of Jennifer Guernsey in manuscript editing.

#### REFERENCES

- (1) Ijesebaert, J. C.; Geerse, K. B.; Marijnissen, J. C. M.; Lammers, J. W. J.; Zanen, P. *J. Appl. Physiol.* **2001**, *91*, 2735–2741.
- (2) De La Mora, J. F.; Navascues, J.; Fernandez, F.; Rosell-Llompart, J. *Aerosol. Sci.* **1990**, *21*, 673–676.
- (3) Ebeling, D. D.; Westphall, M. S.; Scalf, M.; Smith, L. M. *Anal. Chem.* **2000**, *72*, 5158–5161.
- (4) Qi, Lu; Koropchak, J. A. *Anal. Chem.* **2004**, *76*, 5539–5546.
- (5) Camelot, D.; Marijnissen, J. C. M.; Scarlett, B. *Ind. Eng. Chem. Res.* **1999**, *38*, 631–638.
- (6) Almekinders, J. C.; Jones, C. *J. Aerosol. Sci.* **1999**, *30*, 969–971.
- (7) Frey, B. L.; Lin, Y.; Westphall, M. S.; Smith, L. M. *J. Am. Soc. Mass Spectrom.* **2009**, *16*, 1876–1887.
- (8) Xie, J.; Lim, L. K.; Phua, Y.; Hua, J.; Wang, C. H. *J. Colloid Interface Sci.* **2006**, *302*, 103–112.
- (9) Bacher, G.; Szymanski, W. W.; Kaufman, S. L.; Zöllner, P.; Blaas, D.; Allmaier, G. *J. Mass Spectrom.* **2001**, *36*, 1038–1052.
- (10) Scalf, M.; Westphall, M. S.; Krause, J.; Kaufman, S. L.; Smith, L. M. *Science* **1999**, *283*, 194–197.
- (11) Welle, A. M.; Jacobs, H. O. *Appl. Phys. Lett.* **2005**, *87*, 263119.
- (12) Morozov, V. N. *J. Aerosol. Sci.* **2011**, *42*, 341–354.
- (13) Seymour, J. L.; Syrstad, E. A.; Langley, C. C.; Turecek, F. *Int. J. Mass Spectrom.* **2003**, *228*, 687–702.
- (14) Pittier, S. J.; McLuckey, S. A. *Mass Spectrom. Rev.* **2005**, *24*, 931–958.
- (15) Morozov, V. N.; Morozova, T. Ya. *Anal. Chem.* **1999**, *71*, 1415–1420.
- (16) Liu, W. R.; Langer, R.; Klibanov, A. M. *Biotechnol. Bioeng.* **1991**, *37*, 177–184.
- (17) Mazo, M. A.; Manevitch, L. I.; Gusarova, E. B.; Shamaev, M. Yu.; Berlin, A. A.; Balabaev, N. K.; Rutledge, G. C. *J. Phys. Chem. B* **2008**, *112*, 3597–3604.
- (18) Glyakina, A. V.; Balabaev, N. K.; Galzitskaya, O. V. *J. Chem. Phys.* **2009**, *131*, 045102.
- (19) Wang, J.; Cieplak, P.; Kollman, P. A. *J. Comput. Chem.* **2000**, *21*, 1049–1074.
- (20) Jorgensen, W. L.; Chandrasekhar, J.; Madura, J. D.; Impey, R. W.; Klein, M. L. *J. Chem. Phys.* **1983**, *79*, 926–935.
- (21) Lemak, A. S.; Balabaev, N. K. *Mol. Simul.* **1995**, *15*, 223–231.
- (22) Lemak, A. S.; Balabaev, N. K. *J. Comput. Chem.* **1996**, *17*, 1685–1695.
- (23) Allen, M. P.; Tildesley, D. J. *Computer Simulations of Liquids*; Clarendon Press: Oxford, U.K., 1987.

- (24) Schnier, P. D.; Gross, D. S.; Williams, E. R. *J. Am. Soc. Mass Spectrom.* **1995**, *6*, 1086–1097.
- (25) Reimann, C. T.; Velazquez, L.; Tapia, O. *J. Phys. Chem. B* **1998**, *102*, 9344–9352.
- (26) de la Mora, J. F. *Anal. Chim. Acta* **2000**, *406*, 93–104.
- (27) Sheu, S. Y.; Yang, D. Y. *J. Phys. Chem. B* **2010**, *114*, 16558–16566.
- (28) Morozov, V. N.; Morozova, T. Y.; Kachalova, G. S.; Myachin, E. T. *Int. J. Biol. Macromol.* **1988**, *10*, 329–336.
- (29) Nagato, K.; Matsui, Y.; Miyata, T.; Yamauchi, T. *Int. J. Mass Spectrom.* **2006**, *248*, 142–147.
- (30) Sekimoto, K.; Takayama, M. *Int. J. Mass Spectrom.* **2007**, *261*, 38–44.
- (31) Hvelplund, P.; Kadane, U.; Nielsen, S. B.; Panja, S.; Stochkel, K. *Int. J. Mass Spectrom.* **2010**, *292*, 48–52.
- (32) Ahadi, E.; Konermann, L. *J. Am. Chem. Soc.* **2011**, *133*, 9354–9363.
- (33) Krieger, E.; Koraimann, G.; Vriend, G. *Proteins* **2002**, *47*, 393–402.
- (34) Marklund, E. G.; Larsson, D. S. D.; van der Spoel, D.; Patriksson, A.; Caleman, C. *Phys. Chem. Chem. Phys.* **2009**, *11*, 8069–8078.
- (35) Breukera, K.; McLafferty, F. W. *Proc. Natl. Acad. Sci. U.S.A.* **2008**, *105*, 18145–18152.
- (36) Consta, S. *J. Phys. Chem. B* **2010**, *114*, 5263–5268.
- (37) Znamenskiy, V.; Marginean, I.; Vertes, A. *J. Phys. Chem. A* **2003**, *107*, 7406–7412.
- (38) Ahadi, E.; Konermann, L. *J. Am. Chem. Soc.* **2010**, *132*, 11270–11277.
- (39) Sundén, A. E. K.; Stochkel, K.; Panja, S.; Kadane, U.; Hvelplund, P.; Brøndsted, S.; Zettergren, H.; Dynefors, B.; Hansen, K. *J. Chem. Phys.* **2009**, *130*, 224308.
- (40) Sturtevant, J. M. *Proc. Natl. Acad. Sci. U.S.A.* **1977**, *74*, 2236–2240.
- (41) Hinz, H.-J.; Vogl, T.; Meyer, R. *Biophys. Chem.* **1994**, *52*, 275–285.
- (42) Bukatina, A. E.; Morozov, V. N.; Gusev, N. B.; Sieck, G. C. *FEBS Lett.* **2002**, *524*, 107–110.
- (43) Tureček, F. *J. Am. Chem. Soc.* **2003**, *125*, 5954–5963.
- (44) Takats, Z.; Drahos, L.; Schlosser, G.; Vekey, K. *Anal. Chem.* **2002**, *74*, 6427–6429.
- (45) Olumee, Z.; Callahan, J. H.; Vertes, A. *J. Phys. Chem. A* **1998**, *102*, 9154–9160.
- (46) Venter, A.; Sojka, P. E.; Cooks, R. G. *Anal. Chem.* **2006**, *78*, 8549–8555.
- (47) Ivanov, A. V.; Trakhtenberg, S.; Bertram, A. K.; Gershenson, Y. M.; Molina, M. *J. Phys. Chem. A* **2007**, *111*, 1632–1637.